ISSN 1330-3651 (Print), ISSN 1848-6339 (Online) https://doi.org/10.17559/TV-20240508001530
Original scientific paper

Advancements in Efficient Underwater Image Restoration Using ETransMapNet for Enhanced Dehazing

C. P. INDUMATHI, HAYA MESFER ALSHAHRANI, NATRAJ N. A.*, C. H. SARADA DEVI

Abstract: Underwater (UW) information is essential for advancing human exploration and utilization of the underwater world, including fields such as UW Paleology, UW Target Detection, UW Object Tracking, UW Surveillance, and related activities. Visual media like movies and images enhance our natural understanding of underwater objectives. In the past decade, underwater photo restoration and enhancement have gained increasing attention. This study proposes a novel approach employing the recently developed Convolutional Neural Network (CNN) for dehazing, named ETransMapNet (Efficient Transmission Map Network). ETransMapNet is designed with convolution layers and nonlinear activations to execute four sequential processes: nonlinear regression, local maxima detection, multi-scale decomposition, and convolutional feature extraction. Unlike traditional CNNs, ETransMapNet replaces the initial layer's Rectified Linear Unit (ReLU) activation with a convolution layer utilizing a Maxout activation function. ETransMapNet extracts features using three convolution kernels of different sizes (3 × 3, 5 × 5, and 7 × 7). The method suppresses noise in the estimated transmittance map, while local extremum values maintain local consistency within the transmittance map. This study adopts Bilateral ReLU (BReLU) for normalizing network outputs within a 0 to 1 range. Additionally, Adaptive Bilateral Filtering (ABF) is applied to remove redundant artifacts from the predicted transmission map. White balancing addresses color divergence, and Laplacian pyramid fusion combines the color-corrected and dehazed images. In the final stage, the resultant image is transformed into the Wavelet and Directional Filter Banks (WDFB) domain for denoising and edge enhancement. Performance metrics reveal that the proposed ETransMapNet approach improves performance by 38% - 50% compared to previous methods.

Keywords: Adaptive Bilateral Filtering (ABF); Convolutional Neural Network (CNN); ETransMapNet; transmission map denoising; underwater image restoration

1 INTRODUCTION

Underwater vision has become an essential tool for investigating the marine environs. When it comes to giving underwater robots the information they need to perform a variety of tasks, including underwater photography, underwater exploration, underwater rescue, and marine archaeology, high-quality underwater photos are essential. Nevertheless, because of light absorption and dispersion, underwater photos are vulnerable to color falsification, squat contrast, and gesticulation blur. Consequently, improving underwater optical image quality has emerged as a key area of study for Image to Image data processing (Computer Vision) and ocean engineering. Researchers and specialists have worked hard to improve underwater images during the past couple of decades. Physical model-based, non-physical model-based , and data-driven approaches are three categories into which different approaches can be divided. In order to capture distinct pictures of underwater, physical model techniques estimate the variable parameters of the image establishment model and consider underwater image enhancement as an inverse problem. The dark channel prior (DCP) model, which includes the underwater DCP [1] and generalized DCP [2], is one of the most used techniques.

In different water locations, the degree of degradation varies depending on the water contents [3]. Although improving these low-quality underwater images has shown to be a difficult precondition for underwater object detection, monocular depth estimation, and underwater object tracking, the increased visibility can highlight scenes and objects more [4].

The particles in the medium absorb and scatter the underwater object's reflected light, resulting in low-contrast images that are often captured by the camera. Color constancy comes in second. Since long waves absorb light more readily than short ones [5], underwater photos typically have a bluish or greenish tint [6]. Thus, color cast correction and contrast improvement are the main goals of underwater image enhancement (UIE) algorithms [7]. Many techniques have been put out recently to improve underwater images. In general, there are three types of UIE approaches: data-driven deep learning methods, physical prior-based methods, and classical methods that do not explicitly develop models.

Hence, we proposed an innovative UW image enhancement technique using deep learning architecture of ETransMapNet in this paper. The adaptive and effective Transmission Map (TM) prediction is done with this network by integrating the Maxout activation and BilateralReLU in the deep learning of regression of transmission map. After this stage 1, the enhanced image should be influenced with color correction and edge preservation for sharpness maintenance in the image. Color correction is performed using Weighted Multi-Scale-Pyramid Fusion (WMSPF) and edge preservation is solved by integrating wavelet and directional filter bank for decomposition based local and global information restoration in the image to achieve the final stage of underwater image enhancement.

2 LITERATURE SURVEY

A number of investigators employ sonar and optical hardware technologies, such as multi-beam sonar [8], range-gated imaging [9], polarization imaging [10], and range-gated imaging [11], to obtain data underwater. Certain dehazing techniques have been developed to deblur underwater photos because the corporeal model of murkiness imaging is similar to that of underwater imaging [12]. The novelist [13] suggested guided filter and soft similarity as ways to improve the transmission map following the Dark Channel Prior hypothesis. Certain areas of the image appear as haloes that cover the features for the reason that the TM is computed depending on the image patches and the section.

The fundamentals of several activities for improving underwater images and contrasting their outcomes.

Underwater image deblurring and underwater image color correction are the two categories into which they separated underwater image enhancing techniques. Underwater image enhancement techniques are separated into two categories by our research: Picture Element based and corporeal model based UW imaging [14]. The new global histogram stretching RGHS approach is one of the image based techniques. In order to improve the image quality, RGB and CIElab color spaces of image are utilized for stretching the histogram.

The physical model of underwater imaging is the foundation for all of the subsequent techniques. The introduction of the deep learning [15] approach makes a difference. A different prior model of ULAP to estimate the model factors, transmission, and background light based on the physical model of underwater photographs.

The different color space ratio model as blue-red to blue-green light of attenuation. From the conventional image defogging solution, UW image deblurring is implemented by considering the attenuation of multiple light of multiple wavelengths in different water surface [16]. Since the target scene's water quality type is unknown, the study uses the light attenuation coefficients of all known water quality types to produce a variety of restoration images with varying effects.

While GAN seeks to enhance the image's perceived quality, CNN seeks to remain true to the original underwater image. CNN performs exceptionally well in image-based tasks [17]. Based on CNN, several well-known deep neural network frameworks are used for low-level pictures, low-light image improvement, image denoising, and image de-blurring. The approach that calculates spatio temporal perspective weight is dubbed adaptive spatial-temporal context-aware by the authors. The technique may be used to track many creature species in an aquatic environment [18].

In their learning approach, the retinex method introduced a retinex decomposition with deep learning network to improve UW image [19]. The scientists evaluated the lighting using a Convolutional Neural Network for the reference point model and concentrated on enhancing the color, contrast, and brightness. The authors employed RGB and HSV color representations to create an E2E network using convolutional neural networks [20-22]. They also employed piece-wise-linear scaling, which facilitates understanding HSV features.

The research gap lies in effectively addressing underwater image dehazing, deblurring, and color correction under varying water conditions using traditional methods, which often fail to adapt to diverse environments. Recent advancements in deep learning, such as CNN and GAN-based approaches, have shown promise in enhancing image quality, but challenges remain in balancing image fidelity and perceptual enhancement. The proposed solutions focus on leveraging advanced neural networks, like adaptive spatial-temporal models and retinex-based decomposition, to improve image clarity and color correction in dynamic underwater scenarios.

3 THE PROPOSED METHOD

Previous image-based research In order to recover the clean underwater photos, UIE has concentrated on obviously exhibiting the underwater deterioration model and approximating the model factors from the scrutiny and different priors. The traditional Jaffe–McGlamery model that served as the basis for the physical underwater imaging concept is expressed as follows:

$$I^C(p) = J^C(p) + T^C(p) + A^C\left(1 - T^C(p)\right),\ c \in \{r, g, b\} \quad (1)$$

where $I^C(p)$ is underwater image, $J^C(p)$ is original image to be restored and c is color space of R, G, B. For restoration, global background light A^C and the transmission matrix T^C are the key parameters. Most researchers worked on these parameters such as underwater DCP, RCP, and adaptive ACP. Unambiguously, the subsequent formula can be resulting from Eq. (1).

$$\begin{aligned} J_C(x) &= \left(\left(I_C(x) - A^C\right)\right)\Big/ t(x) + A^C = \\ &= \left(I_C(x) - \left(A^C\left(1 - t(x)\right)\right)\right)\Big/ t(x) \end{aligned} \quad (2)$$

By influencing the information enclosed in the dark channel, precise estimates of A^C of the image can be obtained by.

$$J_{dark}(x) = \underset{c \in \{r, g, b\}}{\mathrm{main}} \left\{ \min_{y \in \Omega(x)} j_c(x) \right\} \quad (3)$$

While DCP works well for processing images on land, its immediate use in an underwater context performs poorly. As a result, the UDCP-a DCP variant is presented. An compute dark channels and estimate transmission by ignoring the red channel and relying only on the data from the blue and green channels. Background light A^C can be derived.

$$A^c(x) = I^C\left(\mathrm{argmax} J_{dark}(x)\right),\ x \in P_{0.1\%},\ C \in \{g, b\} \quad (4)$$

In the R-color space of resultant image, 0.1% of upper intensity pixels i.e., 255 values of pixels are exploited as the background light of R-channel and it is articulated as

$$A^c(x) = I^C(x),\ x \in P_{0.1\%},\ C \in \{r\} \quad (5)$$

The final restored image is recuperated by:

$$J(x) = \frac{I^C(x) - A^C(x)}{max\left(t_0, t(x)\right)} + A^C(x),\ C \in \{r, g, b\} \quad (6)$$

where emblematic value of t_0 is 0.1. Nevertheless, underwater photos with less considerable color departure are not susceptible to this straightforward and efficient prior based on the prior understanding that during imaging things at greater distances get more hazy. Conventional models cannot correctly determine the real transmission map if the input image is severely distorted. Therefore, as shown in the sections that follow, we suggested the efficient transmission map estimate utilizing a unique deep learning architecture.

In this UW enhancement system, the transmission map is estimated using a novel deep learning architecture named ETransMapNet. The TM is refined by integrating artifact removal function of adaptive bilateral filter (ABF). Enhanced image at this stage 1 is obtained by the underwater image model with the value of background light which is predicted from the input underwater image. For stage 2 enhancement we used three techniques named as white balance for color correction, laplacian pyramid fusion for fusion of these two images and Wavelet Directional Filter Bank (WDFB) for edge preservation.

When inputs are negative, the ReLU function saturates. Gradient diffusion occurs in these saturation zones, preventing gradients from moving down to deeper layers. ReLUs may also die out during learning, which would prevent error gradients from being learned and result in nothing being learned . Various activation functions have been suggested for DNN training due to these reasons. Combining the maxout nonlinearity through dropout, which is recurrently applied to standardize DNN to minimize overcompensate, allows for the selection of the largest value among a range of distinct outputs (feature maps). The entire blockdiagram of the proposed is shown in Fig. 1.

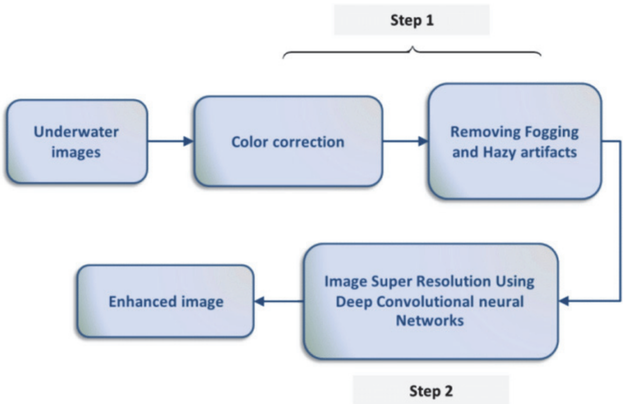

Figure 1 Proposed underwater Image enhancement block diagram

Our model trains the activation function known as the Maxout unit. One way to think about a single Maxout unit is as a piecewise linear approximation to any convex function as

$$h(x) = \max(Z_1, Z_2, Z_3, ..., Z_n) \tag{7}$$

$$h(x) = \max(W_1 \cdot x + b_1, W_2 \cdot x + b_2, ..., W_n \cdot x + b_n) \tag{8}$$

Z represents the lineal pre-activation value; n and j stand for the number of maxout units and pre-activation values, respectively; b and w denote the bias and weight of each activation. In a network, maxout selects the extreme of n input characteristics to generate each output feature. The suggested ETransMapNet, with a maxout unit in a CNN design and a $N \times N$ pixel picture for Y, is seen in Fig. 2. The maximum rate of the convolution operations on $y1$, $y2$, and $y3$ is taken by the maxout unit. CNN picks up on the bias and weights in the $F1$, $F2$, and $F3$ filters. In order to keep units from overfitting, dropout randomly removes connections or units. The nonlinear regression function with max pooling and bilateral ReLU is denoted as $F(Y)$.

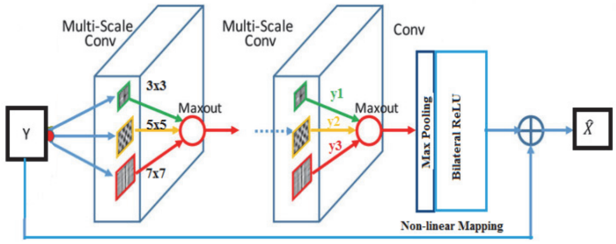

Figure 2 Proposed ETransMapNet Deep Learning Layer Architecture

The BReLU function is given by:

$$f(y) = \min(t_{\max}, \max(t_{\min}, y)) \tag{9}$$

In Eq. (9), $t_{\max}$ and $t_{\min}$ are the marginal constant values for BReLU. In BReLU, $t_{\min}$ and $t_{\max}$ are the constant values with $t_{\min} = 0$ and $t_{\max} = 1$, respectively. Fig. 4 demonstrates the convergence graph of the BReLU. To enhance the convergence performance, BReLU is reducing the search space by application of bi-directional constraints.

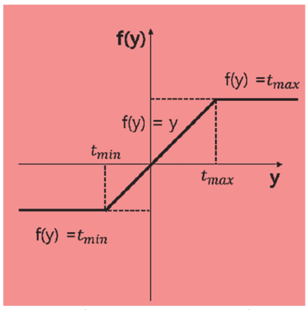

Figure 3 Convergence curve of BreLU

Adaptive Bilateral Filter.

The image's false-color textures may be effectively removed using the Gaussian filter, but the image's edges are also blurred, causing information to be missed. The bilateral filter technique blurs the picture while maintaining the edge information. Weighted nearby pixels are used. Higher weights are assigned to the pixels that are closest to the central pixel. As a result, the boundaries of the transmission map are preserved but become blurry. Compared to the map produced by the Gaussian filter, the improved map produced by the bilateral filter contains more precise information. Quantitative performance-wise, this is ineffective as the range kernel's standard deviation rises with the root mean square. The bilateral filter can be represented in Eq. (10).

In this instance, x represents the center pixel location, y the current pixel coordinate, and G_{σ_s} and G_{σ_r} can be Gaussian functions with σ_s and σ_r, respectively, for standard deviations. The spatial kernel used to smooth location disparities is called G_{σ}. A weighted average of the local pixel intensities can be used to represent the conventional bilateral filter, as was noted in . We apply the same principle to the bilateral adaptive filter. An adaptive version of the bilateral filter was shown, allowing the Gaussian range kernel's width and center to vary from pixel to pixel. It was applied to both noise reduction and picture sharpness enhancement. Since sharpening cannot be achieved with the conventional bilateral filter, the range kernel had to be adjusted. By adjusting the kernel's width and center, the degree of noise reduction and sharpness at a specific pixel may be adjusted.

Let $f: I \rightarrow \mathbb{R}$ be the input image, where $I \subset \mathbb{Z}^2$ is the image domain. The output image $g: I \rightarrow \mathbb{R}$ is given by.

$$g(i)=\eta(i)^{-1} \sum_{j \in \Omega} \omega(j) \phi_i\left(f(i-j)-\theta(i)\right) f(i-j) \tag{11}$$

where

$$\eta(i)=\sum_{j \in \Omega} G_{\sigma_r} \phi_i\left(f(i-j)-\theta(i)\right) \tag{12}$$

Here is a window centered at the origin, and ϕ_i is the local Gaussian range kernel and it is given by Eq. (13).

$$\phi_i(t)=\exp\left(-\frac{t^2}{2\sigma(i)^2}\right) \tag{13}$$

Prominently, the midpoint $\theta(i)$ in Eq. (11) and the width $\sigma(i)$ in Eq. (13) are spatially capricious functions. The spatial kernel $\omega: \Omega \rightarrow \mathbb{R}$ in Eq. (11) is Gaussian as:

$$\omega(t)=\exp\left(-\left(\frac{\left\|j^2\right\|^2}{2\rho^2}\right)\right) \tag{14}$$

The frame is stereotypically fixed to square of negative 3ρ to positive 3ρ for Ω.

The filter is performing the σ_r selection spontaneously by computing the variance of image blocks σ_{blk} along with consideration of ranges. It can be represented as:

$$\sigma_r=\max\left(\sigma_{r,\min}, \min\left(\sigma_{r,\max}, k\sigma_{blk}\right)\right) \tag{15}$$

where maximum range and minimum range are denoted as $\sigma_{r,\min}$ and $\sigma_{r,\max}$ respectively, and k is integer constant. In this work, we assign $\sigma_{r,\min}=1$, $\sigma_{r,\max}=10$, $k=6$.

Fig. 4 displays the decomposition diagram of WDFB. In high-frequency subbands where texture and contour features are more abundant, the WDFB transform's coefficients are greater than those of the traditional DWT transform. The noise variance of the input picture is estimated using the first layer's high-frequency coefficients. The threshold T_k may then be obtained by using the denoising preprocessing based on the wavelet threshold approach as,

$$T_k=\frac{1}{2}\sqrt{\frac{1}{m \times n}\sum_{x=1}^{m}\sum_{y=1}^{n}\left[P_k(x,y)-\overline{P}\right]^2} \tag{16}$$

where $\overline{P}$ is the average of the WDFB factors in leading layer. Noise is defined as coefficients less than the threshold. The coefficients that exceed the threshold are considered to have fuzzy edges. Blurred edges E_i drops to zero by multiplying the WDFB decomposed layer coefficients of HHi, LHi, and HLi.

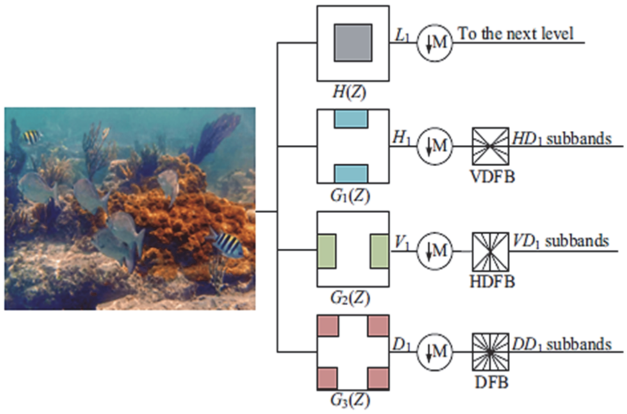

Figure 4 Wavelet and directional filter bank decomposition

3 RESULTS AND DISCUSSION

To evaluate the enactment of the proposed method, assessments are carried out against several earlier deep learning works of underwater image enhancement methods, such as Water-Net [25], Shallow-Uwnet [45], Nested ResNet [46], UimageFitNet [47], Ucolor [48], LightCasNet [49], PUIEnet [50]. To substantiate the effectiveness of our proposed ETransMapNet based enhancement of underwater (UW) image, we considered six different datasets named as EUVP, SQUID, UIEBD, RUIE-UIQS, RUIE-UCCS and U-45. For Quantitative Analysis, we considered multiple metrics for comparison using Simulation in the platform of MATLAB 2020a version.

An extensive assemblage of unpaired and paired underwater photos with capricious levels of perceptual eminence is established in the EUVP dataset. The information was congregated in sundry places with erratic perceptibility situations during supportive human-robot examinations and marine excursions. This dataset comprises around 8000 unpaired and 12000 paired cases.

The SQUID dataset is collected in situ data in a variety of water types, seasons, and depths (both in murkier coastal waters and tropical regions). The only lighting used in each scene was natural light. RAW photos, TIF files, camera calibration files, and distance maps are all included in the SQUID dataset. There are 57 stereo pairs in the collection from four distinct locations in Israel: two in the Mediterranean Sea (which represents temperate water) and two in the Red Sea (which represents tropical water). The locations were a shipwreck called "Satil," which was 20 - 30 meters deep, and a coral reef called "Katzaa," which was 10 - 15 meters deep (15 pairs). Fig. 8 demonstrates how we applied our suggested strategy to improve underwater photos from the SQUID dataset.

An efficient and widely available UWdatabase that captures the color troupes, deprived disparity, and fog appearance possessions of UW deterioration is the U45 database. The U45 dataset is divided into 3 categories:

blue, green and both. Since the other three groups include a variety of low contrast underwater photos, they did not only set a low contrast data set. The UIEB Dataset is divided into two subsets: 60 difficult underwater photos and 890 underdone underwater images paired with matching top quality reference photographs. These are actual underwater photos that were shot in a variety of lighting conditions, including artificial, natural, and a combination of both. UIEB offers a wide variety of scene/main object categories and a wide range of picture resolutions, such as coral (such as barrier and bordering reefs), marine life (such as sharks and turtles), etc. To show the different range and regions of underwater image performance using our algorithm with this UIEB dataset is revealed in Fig. 7.

Figure 5 Proposed ETransMapNet based underwater enhancement for EUVP dataset

Adaptive Bilateral Filtering effectively minimizes artifacts, enhancing underwater image clarity and quality.

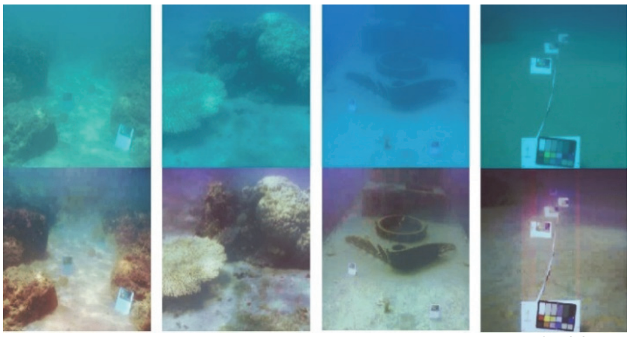

Figure 6 Proposed ETransMapNet based underwater enhancement for SQUID dataset

The integration of Maxout activation in ETransMapNet improves feature extraction by allowing more flexible and effective non-linear mappings compared to traditional ReLU, leading to better performance

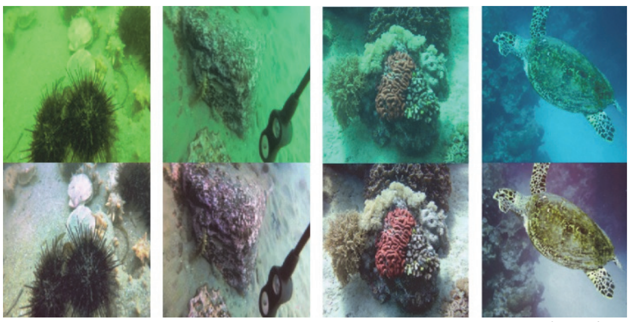

Figure 7 Proposed ETransMapNet based underwater enhancement for U-45 dataset

Figure 8 Proposed ETransMapNet based underwater enhancement for UIEBD dataset

Performance Evaluation Index.

The *PSNR*, or peak possible signal power to distorting noise power ratio, gauges how well a signal is represented. One may compute *PNSR* using the maximum pixel range of *L* as follows:

$$PSNR = 10\log_{10}\frac{L^2}{MSE} \tag{17}$$

Three elements are taken into account by *SSIM*: local structures $s(x, y)$, contrasts $c(x, y)$, and the similarity of the patch luminance $l(x, y)$. *SSIM* is as follows:

$$SSIM = l(x,y)\cdot c(x,y)\cdot s(x,y) \tag{18}$$

Depending on their wavelength, colors weaken one by one as the water's depth rises. Because red has the shortest wavelength of all the colors, it vanishes earliest. Consequently, photos taken underwater typically have a blue or greenish tint. Moreover, extreme color de-saturation in underwater photos is also caused by inadequate illumination. A decent algorithm for enhancing underwater photos should result in well-defined colors. Colors in the antagonist's color plane are apprehended by the HVS. As a result, as demonstrated in, the double antagonist color constituents connected with chrominance are utilized in the *UICM* given by,

$$RG = R - G \tag{19}$$

$$YB = \frac{R+G}{2} - B \tag{20}$$

Images taken underwater typically include a lot of noise. Consequently, the irregular alpha sheared numerical values are employed to measure the colorfulness of underwater images instead of the standard statistical values. The mean is defined by:

$$\mu_{\alpha,RG} = \frac{1}{K - T_{\alpha L} - T_{\alpha R}}\sum_{i=T_{\alpha L}+1}^{K-T_{\alpha R}} Intensity_{RG,i} \tag{21}$$

The second-order statistic variance given by:

$$\sigma^2{}_{\alpha,RG} = \frac{1}{N}\sum_{p=1}^{N}\left(Intensity_{RG,i} - \mu_{\alpha,RG}\right)^2 \tag{22}$$

UICM is given as:

$$UICM = -0.0268\sqrt{\mu_{\alpha,RG}^2 + \mu_{\alpha,YB}^2} + 0.1586\sqrt{\sigma_{\alpha,RG}^2 + \sigma_{\alpha,YB}^2} \quad (23)$$

The quality associated with maintaining little details and edges is sharpness. Forward scattering causes significant blurring in photos taken underwater. The clarity of the image is decreased by this blurring effect. Only the margins of the original underwater picture are kept while doing this. It is well known that photographs with a uniform backdrop and non-periodic patterns can benefit from the enhancement measure estimation (*EME*) metric, which is used to gauge how sharply edges are defined. The *UISM* is formulated as,

$$UISM = \sum_{c=1}^{3} \lambda_c EME\left(edge_c\right) \quad (24)$$

$$EME = \frac{2}{k_1 k_2} \sum_{l=1}^{k_1} \sum_{k=1}^{k_2} log\left(\frac{I_{\max,k,l}}{I_{\min,k,l}}\right) \quad (25)$$

where k_1, k_2 are the two blocks separated from the image.

Underwater visual performance, including stereoscopic acuity, has been demonstrated to correlate with contrast. Backward scattering is typically to blame for contrast reduction in underwater photos. *UIConM* is given by:

$$UIConM = \log AMEE\left(Intensity\right) \quad (26)$$

$$\begin{aligned} \log AMEE = \frac{1}{k_1 k_2} \otimes \\ \otimes \sum_{l=1}^{k_1} \sum_{k=1}^{k_2} \frac{I_{\max,k,l} - I_{\min,k,l}}{I_{\max,k,l} + I_{\min,k,l}} \times \log\left(\frac{I_{\max,k,l} - I_{\min,k,l}}{I_{\max,k,l} + I_{\min,k,l}}\right) \end{aligned} \quad (27)$$

High *UIQM* value indicates high human visual perception in the given image. *UIQM* can be calculated as follows:

$$UIQM = c1 \cdot UICM + c2 \cdot UISM + c3 \cdot UIConM \quad (28)$$

The selections of $c1$, $c2$ and $c3$, parameters are application dependent. For the results shown in this paper, a generic coefficient set, $c1$ = 0.0282, $c2$ = 0.2953 and $c3$ = 3.573 is used. In our enhancement of UW images, compared with color, contrast and sharpness are the most impact factors.

Table 1 Proposed ETransMapNet based underwater enhancement

Metrics Methods	*PSNR* (dB) ↓	*SSIM* ↓	*UICM* ↑	*UISM* ↑	*UIConM* ↑	*UIQM* ↑	*FDUM* ↑	*UICQE* ↑
Water-Net	24.13	0.8804	10.26	4.86	2.56	1.35	0.51	0.57
Shallow-UWnet	22.24	0.8921	11.66	6.02	3.17	1.43	0.63	0.70
Nested ResNet	21.73	0.8533	10.55	5.26	3.02	1.56	0.60	0.64
UImageFitNet	20.62	0.8117	12.19	5.86	3.41	1.77	0.64	0.71
UColor	19.77	0.7695	12.29	6.27	3.45	1.81	0.78	0.83
LightCasNet	19.65	0.6741	10.67	6.05	3.41	1.96	0.76	0.68
PUIEnet	18.35	0.6216	11.43	6.87	3.58	2.12	0.79	0.75
Proposed ETransMapNet	15.91	0.5811	14.09	8.98	5.72	4.39	0.86	0.89

In underwater image, absorption and scattering attain the main effective cause. Colorfulness is affected by absorption, contrast by backscattering and sharpness by scattering. Thus, Frequency Domain Underwater Measurement (*FDUM*) metric is obtained by fusing the contrast, sharpness and colorfulness values by:

$$FDUM = \omega 1 \cdot Sharpness + \omega 2 \cdot Contrast + \omega 3 \cdot Colorfulness \quad (29)$$

where ω1, ω2 and ω3 are the weights of sharpness, contrast, and colorfulness measurements, respectively. In our method, the coefficients are fixed as [0.028, 0.4439, 0.2982].

For evaluation of this metric, the RGB image I is converted to CIELab color space L. The image L is represented as $L(i, j) = [l(i, j)\ a(i, j)\ b(i, j)]$. All the pixels are reshaped to vector as N pixel values. CI is the chroma [14]. The Underwater Colour Image Quality Evaluation (UCIQE) metric of image I is represented as,

$$UCIQE = c1 \cdot \sigma_c + c2 \cdot C_L + c3 \cdot S_A \quad (30)$$

where, σ_c is the chroma's standard deviation, S_A is the mean of saturation and C_L is the contrast of luminance, and $c1$, $c2$, $c3$ are weights. In this work, let $c1$ = 0.4680, $c2$ = 0.2745, $c3$ = 0.2576 for the equivalent measures.

The performance comparison of the proposed ETransMapNet based underwater Image enhancement is compared for different metrics of above mentioned with the earlier works of the same with deep learning algorithms. The 38% - 50% performance improvement demonstrates the effectiveness of the proposed approach, showcasing its significant potential in enhancing underwater imaging applications.

5 CONCLUSION

Three processes are involved in the underwater picture improvement suggested in this paper: edge enhancement, color enhancement, and efficient transmission map prediction. The adaptive Transmission map with contrast deviation correction is generated by using the ETransMapNet. The ETransMapNet deep learning architecture's bilateral ReLU contributes to the development of the improved transmission map of the color underwater picture. White balancing with weighted multiscale pyramid fusion is used to improve color. WDFB is used to accomplish edge preservation, which adds extra information. Extensive qualitative and quantitative tests conducted on publicly accessible underwater datasets demonstrate the great superiority and broad applicability of our approach. The suggested quantitative indicators surpass previous efforts in the same application and deep learning area by 38% to 50%. Although the contrast and color performance of our suggested method is good, there is a chance that noise deviation and noise augmentation will remain unresolved. We intend to investigate these problems in further studies.

Acknowledgments

Princess Nourah bint Abdulrahman Universit Researcher Supporting Project number (PNURSP2025R237), Princess Nourah bint Abdulrahman University, Riyadh, Saudi Arabia.

6 REFERENCES

[1] Lore, K. G., Akintayo, A., & Sarkar, S. (2017). LLNet: A deep autoencoder approach to natural low-light image enhancement. *Pattern Recognition, 61*, 650-662. https://doi.org/10.1016/j.patcog.2016.09.034

[2] Li, C., Guo, J., & Guo, C. (2018). Emerging from water: Underwater image color correction based on weakly supervised color transfer. *IEEE Signal Processing Letters, 25*(10), 1550-1554. https://doi.org/10.1109/LSP.2018.2866619

[3] Akkaynak, D. &Treibitz, T. (2019). Sea-Thru: A method for removing water from underwater images. *IEEE/CVF Conference on Computer Vision and Pattern Recognition (CVPR)*. https://doi.org/10.1109/CVPR.2019.00465

[4] Rizzi, A., Gatta, C., & Marini, D. (2002). Color correction between gray world and white patch. *Human Vision and Electronic Imaging VII, 4662*, 367-375. https://doi.org/10.1117/12.474772

[5] Lan, Z., Zhou, B., Zhao, W., & Wang, S. (2023). An optimized GAN method based on the que-attn and contrastive learning for underwater image enhancement. *PLoS One, 18*, e0279945. https://doi.org/10.1371/journal.pone.0279945

[6] Liu, R., Fan, X., Zhu, M., Hou, M., & Luo, Z. (2020). Real-world underwater enhancement: Challenges, benchmarks, and solutions under natural light. *IEEE Transactions on Circuits and Systems for Video Technology, 30*(12), 4861-4875. https://doi.org/10.1109/TCSVT.2019.2956368

[7] Han, P., Liu, F., Wei, Y., & Shao, X. (2020). Optical correlation assists to enhance underwater polarization imaging performance. *Optics and Lasers in Engineering, 134*, 106256. https://doi.org/10.1016/j.optlaseng.2020.106256

[8] Feng, F., Wu, G., Wu, Y., Miao, Y., & Liu, B. (2020). Algorithm for underwater polarization imaging based on global estimation. *Acta Optica Sinica, 40*(21), 75-83. https://doi.org/10.3788/AOS20204021.2075

[9] Jin-ge, G., Yong, Z., Yong-qiu, Z., Miao, S., Peng, S., & Chen-yang, X. (2020). Optical polarization imaging for underwater target detection with non-scatter background. *Journal of Measurement Science and Instrumentation, 11*(4), 335–342. https://doi.org/10.1016/j.jmsi.2020.04.006

[10] Herkül, K., Peterson, A., & Paekivi, S. (2017). Applying multibeam sonar and mathematical modeling for mapping seabed substrate and biota of offshore shallows. *Estuarine, Coastal and Shelf Science, 192*, 57-71. https://doi.org/10.1016/j.ecss.2017.03.007

[11] He, K., Sun, J., & Tang, X. (2019). Single image haze removal using dark channel prior. *IEEE Conference on Computer Vision and Pattern Recognition*, Miami, FL, USA. https://doi.org/10.1109/CVPR.2019.00201

[12] He, K., Sun, J., & Tang, X. (2013). Guided image filtering. *IEEE Transactions on Pattern Analysis and Machine Intelligence, 35*(6), 1397–1409. https://doi.org/10.1109/TPAMI.2012.213

[13] Huang, D., Wang, Y., Song, W., Sequeira, J., & Mavromatis, S. (2018). Shallow-water image enhancement using relative global histogram stretching based on adaptive parameter acquisition. *International Conference on Multimedia Modeling*, Bangkok, Thailand. https://doi.org/10.1007/978-3-319-73603-7_12

[14] Hu, H., Zhang, Y., Li, X., Lin, Y., Cheng, Z., & Liu, T. (2020). Polarimetric underwater image recovery via deep learning. *Optics and Lasers in Engineering, 133*, 106244. https://doi.org/10.1016/j.optlaseng.2020.106244

[15] Song, W., Wang, Y., Huang, D., &Tjondronegoro, D. (2018). A rapid scene depth estimation model based on underwater light attenuation prior for underwater image restoration. *Pacific-Rim Conference on Multimedia*. Springer, Hefei, China. https://doi.org/10.1007/978-3-030-05710-4_31

[16] Berman, D., Levy, D., Avidan, S., & Treibitz, T. (2021). Underwater single image color restoration using haze-lines and a new quantitative dataset. *IEEE Transactions on Pattern Analysis and Machine Intelligence, 43*(8), 2822-2837. https://doi.org/10.1109/TPAMI.2020.2977335

[17] Li, C., Guo, J., Ren, W., Cong, R., Hou, J., Kwong, S., & Tao, D. (2020). An underwater image enhancement benchmark dataset and beyond. *IEEE Transactions on Image Processing, 29*, 4376-4389. https://doi.org/10.1109/TIP.2020.2982315

[18] Li, L., Pan, J., Lai, W.-S., Lu, X., Yang, M.-H., & Lin, Z. (2019). Blind image deblurring via deep discriminative priors. *International Journal of Computer Vision, 127*(8), 1025-1043. https://doi.org/10.1007/s11263-018-1106-8

[19] Li, C., Anwar, S., & Porikli, F. (2020). Underwater scene prior inspired deep underwater image and video enhancement. *Pattern Recognition, 98*, 107038. https://doi.org/10.1016/j.patcog.2019.107038

[20] Yuan, D., Hu, X., Zhou, B., Zhang, Z., Lin, J., & Zhang, Y. (2022). Learning adaptive spatial-temporal context-aware correlation filters for UAV tracking. *ACM Transactions on Multimedia Computing, Communications, and Applications, 18*(3), 1-18. https://doi.org/10.1145/3472882.3473045

[21] Xu, S., Wu, J., Zheng, X., & Jiang, Y. (2022). Deep retinex decomposition network for underwater image enhancement. *Computers & Electrical Engineering, 100*, 107822. https://doi.org/10.1016/j.compeleceng.2022.107822

[22] Parameswari, A., Bhavani, S., & Kumar, K. V. (2024). A Deep Learning Based Glioma Tumour Detection Using Efficient Visual Geometry Group Convolutional Neural Networks Architecture. *Brazilian Archives of Biology and Technology, 67*. https://doi.org/10.1590/1678-4324-2024230705

Contact information:

C. P. INDUMATHI, Assistant Professor (Sr.Grade)
Department of Computer Science and Engineering,
University College of Engineering,
BIT Campus, Anna University Tiruchirapalli-24, Tamilnadu, India
E-mail: cpindumathi@aubit.edu.in

HAYA MESFER ALSHAHRANI
Department of Information Systems,
College of Computer and Information Sciences,
Princess Nourah Bint Abdulrahman University,
P.O. Box 84428, Riyadh 11671, Saudi Arabia

NATRAJ N. A., Assistant Professor
(Corresponding author)
Symbiosis Institute of Digital and Telecom Management,
Symbiosis International (Deemed University),
Pune, Maharashtra, India
E-mail: natraj@sidtm.edu.in

C. H. SARADA DEVI, Associate Professor
Department of CSE
Meenakshi College of Engineering, India
E-mail: saradhadevi6@gmail.com